Inclusive b decays to wrong sign charmed mesons

J. Abdallah, P. Abreu, W. Adam, P. Adzic, T. Albrecht, T. Alderweireld, R. Alemany-Fernandez, T. Allmendinger, P.P. Allport, U. Amaldi, et al.

EUROPEAN ORGANIZATION FOR NUCLEAR RESEARCH

CERN–EP/2002-089

13 November 2002

Inclusive b Decays to Wrong Sign Charmed Mesons

DELPHI Collaboration

Abstract

The production of wrong sign charmed mesons $b \to \bar{D}_{(s)}X$, $D_{(s)} = (D^0, D^+, D_s)$, is studied using the data collected by the DELPHI experiment in the years 1994 and 1995.
Charmed mesons in $Z \to b\bar{b}$ events are exclusively reconstructed by searching for the decays $D^0 \to K^-\pi^+$, $D^+ \to K^-\pi^+\pi^+$ and $D_s^+ \to \phi\pi^+ \to K^+K^-\pi^+$. The wrong sign contribution is extracted by using two discriminant variables: the charge of the b-quark at decay time, estimated from the charges of identified particles, and the momentum of the charmed meson in the rest frame of the b-hadron.
The inclusive branching fractions of b-hadrons into wrong sign charm mesons are measured to be:

$$\begin{aligned} \mathcal{B}(b \to \bar{D}^0 X) + \mathcal{B}(b \to D^- X) &= (9.3 \pm 1.7(stat) \pm 1.3(syst) \pm 0.4(\mathcal{B}))\% \ , \\ \mathcal{B}(b \to D_s^- X) &= (10.1 \pm 1.0(stat) \pm 0.6(syst) \pm 2.8(\mathcal{B}))\% \end{aligned}$$

where the first error is statistical, the second and third errors are systematic.

(Accepted by Phys. Lett. B)

J.Abdallah[24], P.Abreu[22], W.Adam[50], P.Adzic[11], T.Albrecht[17], T.Alderweireld[2], R.Alemany-Fernandez[8], T.Allmendinger[17], P.P.Allport[23], U.Amaldi[28], N.Amapane[44], S.Amato[47], E.Anashkin[35], A.Andreazza[27], S.Andringa[22], N.Anjos[22], P.Antilogus[26], W-D.Apel[17], Y.Arnoud[14], S.Ask[25], B.Asman[43], J.E.Augustin[24], A.Augustinus[8], P.Baillon[8], A.Ballestrero[45], P.Bambade[20], R.Barbier[26], D.Bardin[16], G.Barker[17], A.Baroncelli[38], M.Battaglia[8], M.Baubillier[24], K-H.Becks[52], M.Begalli[6], A.Behrmann[52], E.Ben-Haim[20], N.Benekos[31], A.Benvenuti[5], C.Berat[14], M.Berggren[24], L.Berntzon[43], D.Bertrand[2], M.Besancon[39], N.Besson[39], D.Bloch[9], M.Blom[30], M.Bluj[51], M.Bonesini[28], M.Boonekamp[39], P.S.L.Booth[23], G.Borisov[21], O.Botner[48], B.Bouquet[20], T.J.V.Bowcock[23], I.Boyko[16], M.Bracko[42], R.Brenner[48], E.Brodet[34], P.Bruckman[18], J.M.Brunet[7], L.Bugge[32], P.Buschmann[52], M.Calvi[28], T.Camporesi[8], V.Canale[37], F.Carena[8], N.Castro[22], F.Cavallo[5], M.Chapkin[41], Ph.Charpentier[8], P.Checchia[35], R.Chierici[8], P.Chliapnikov[41], J.Chudoba[8], S.U.Chung[8], K.Cieslik[18], P.Collins[8], R.Contri[13], G.Cosme[20], F.Cossutti[46], M.J.Costa[49], B.Crawley[1], D.Crennell[36], J.Cuevas[33], J.D'Hondt[2], J.Dalmau[43], T.da Silva[47], W.Da Silva[24], G.Della Ricca[46], A.De Angelis[46], W.De Boer[17], C.De Clercq[2], B.De Lotto[46], N.De Maria[44], A.De Min[35], L.de Paula[47], L.Di Ciaccio[37], A.Di Simone[38], K.Doroba[51], J.Drees[52,8], M.Dris[31], G.Eigen[4], T.Ekelof[48], M.Ellert[48], M.Elsing[8], M.C.Espirito Santo[8], G.Fanourakis[11], D.Fassouliotis[11,3], M.Feindt[17], J.Fernandez[40], A.Ferrer[49], F.Ferro[13], U.Flagmeyer[52], H.Foeth[8], E.Fokitis[31], F.Fulda-Quenzer[20], J.Fuster[49], M.Gandelman[47], C.Garcia[49], Ph.Gavillet[8], E.Gazis[31], T.Geralis[11], R.Gokieli[8,51], B.Golob[42], G.Gomez-Ceballos[40], P.Goncalves[22], E.Graziani[38], G.Grosdidier[20], K.Grzelak[51], J.Guy[36], C.Haag[17], A.Hallgren[48], K.Hamacher[52], K.Hamilton[34], J.Hansen[32], S.Haug[32], F.Hauler[17], V.Hedberg[25], M.Hennecke[17], H.Herr[8], J.Hoffman[51], S-O.Holmgren[43], P.J.Holt[8], M.A.Houlden[23], K.Hultqvist[43], J.N.Jackson[23], G.Jarlskog[25], P.Jarry[39], D.Jeans[34], E.K.Johansson[43], P.D.Johansson[43], P.Jonsson[26], C.Joram[8], L.Jungermann[17], F.Kapusta[24], S.Katsanevas[26], E.Katsoufis[31], G.Kernel[42], B.P.Kersevan[8,42], A.Kiiskinen[15], B.T.King[23], N.J.Kjaer[8], P.Kluit[30], P.Kokkinias[11], C.Kourkoumelis[3], O.Kouznetsov[16], Z.Krumstein[16], M.Kucharczyk[18], J.Lamsa[1], G.Leder[50], F.Ledroit[14], L.Leinonen[43], R.Leitner[29], J.Lemonne[2], V.Lepeltier[20], T.Lesiak[18], W.Liebig[52], D.Liko[50], A.Lipniacka[43], J.H.Lopes[47], J.M.Lopez[33], D.Loukas[11], P.Lutz[39], L.Lyons[34], J.MacNaughton[50], A.Malek[52], S.Maltezos[31], F.Mandl[50], J.Marco[40], R.Marco[40], B.Marechal[47], M.Margoni[35], J-C.Marin[8], C.Mariotti[8], A.Markou[11], C.Martinez-Rivero[40], J.Masik[12], N.Mastroyiannopoulos[11], F.Matorras[40], C.Matteuzzi[28], F.Mazzucato[35], M.Mazzucato[35], R.Mc Nulty[23], C.Meroni[27], W.T.Meyer[1], E.Migliore[44], W.Mitaroff[50], U.Mjoernmark[25], T.Moa[43], M.Moch[17], K.Moenig[8,10], R.Monge[13], J.Montenegro[30], D.Moraes[47], S.Moreno[22], P.Morettini[13], U.Mueller[52], K.Muenich[52], M.Mulders[30], L.Mundim[6], W.Murray[36], B.Muryn[19], G.Myatt[34], T.Myklebust[32], M.Nassiakou[11], F.Navarria[5], K.Nawrocki[51], R.Nicolaidou[39], M.Nikolenko[16,9], A.Oblakowska-Mucha[19], V.Obraztsov[41], A.Olshevski[16], A.Onofre[22], R.Orava[15], K.Osterberg[15], A.Ouraou[39], A.Oyanguren[49], M.Paganoni[28], S.Paiano[5], J.P.Palacios[23], H.Palka[18], Th.D.Papadopoulou[31], L.Pape[8], C.Parkes[23], F.Parodi[13], U.Parzefall[8], A.Passeri[38], O.Passon[52], L.Peralta[22], V.Perepelitsa[49], A.Perrotta[5], A.Petrolini[13], J.Piedra[40], L.Pieri[38], F.Pierre[39], M.Pimenta[22], E.Piotto[8], T.Podobnik[42], V.Poireau[39], M.E.Pol[6], G.Polok[18], P.Poropat[†46], V.Pozdniakov[16], N.Pukhaeva[2,16], A.Pullia[28], J.Rames[12], L.Ramler[17], A.Read[32], P.Rebecchi[8], J.Rehn[17], D.Reid[30], R.Reinhardt[52], P.Renton[34], F.Richard[20], J.Ridky[12], M.Rivero[40], D.Rodriguez[40], A.Romero[44], P.Ronchese[35], E.Rosenberg[1], P.Roudeau[20], T.Rovelli[5], V.Ruhlmann-Kleider[39], D.Ryabtchikov[41], A.Sadovsky[16], L.Salmi[15], J.Salt[49], A.Savoy-Navarro[24], U.Schwickerath[8], C.Schwanda[50], A.Segar[34], R.Sekulin[36], M.Siebel[52], A.Sisakian[16], G.Smadja[26], O.Smirnova[25], A.Sokolov[41], A.Sopczak[21], R.Sosnowski[51], T.Spassov[8], M.Stanitzki[17], A.Stocchi[20], J.Strauss[50], B.Stugu[4], M.Szczekowski[51], M.Szeptycka[51], T.Szumlak[19], T.Tabarelli[28], A.C.Taffard[23], F.Tegenfeldt[48], J.Timmermans[30], L.Tkatchev[16], M.Tobin[23], S.Todorovova[12], A.Tomaradze[8], B.Tome[22], A.Tonazzo[28], P.Tortosa[49], P.Travnicek[12], D.Treille[8], G.Tristram[7], M.Trochimczuk[51], C.Troncon[27], M-L.Turluer[39], I.A.Tyapkin[16], P.Tyapkin[16], S.Tzamarias[11], V.Uvarov[41], G.Valenti[5], P.Van Dam[30], J.Van Eldik[8], A.Van Lysebetten[2], N.van Remortel[2], I.Van Vulpen[30], G.Vegni[27], F.Veloso[22], W.Venus[36], F.Verbeure[2], P.Verdier[26], V.Verzi[37], D.Vilanova[39], L.Vitale[46], V.Vrba[12], H.Wahlen[52],

A.J.Washbrook[23], C.Weiser[17], D.Wicke[8], J.Wickens[2], G.Wilkinson[34], M.Winter[9], M.Witek[18], O.Yushchenko[41], A.Zalewska[18], P.Zalewski[51], D.Zavrtanik[42], N.I.Zimin[16], A.Zintchenko[16], M.Zupan[11]

[1]Department of Physics and Astronomy, Iowa State University, Ames IA 50011-3160, USA
[2]Physics Department, Universiteit Antwerpen, Universiteitsplein 1, B-2610 Antwerpen, Belgium
and IIHE, ULB-VUB, Pleinlaan 2, B-1050 Brussels, Belgium
and Faculté des Sciences, Univ. de l'Etat Mons, Av. Maistriau 19, B-7000 Mons, Belgium
[3]Physics Laboratory, University of Athens, Solonos Str. 104, GR-10680 Athens, Greece
[4]Department of Physics, University of Bergen, Allégaten 55, NO-5007 Bergen, Norway
[5]Dipartimento di Fisica, Università di Bologna and INFN, Via Irnerio 46, IT-40126 Bologna, Italy
[6]Centro Brasileiro de Pesquisas Físicas, rua Xavier Sigaud 150, BR-22290 Rio de Janeiro, Brazil
and Depto. de Física, Pont. Univ. Católica, C.P. 38071 BR-22453 Rio de Janeiro, Brazil
and Inst. de Física, Univ. Estadual do Rio de Janeiro, rua São Francisco Xavier 524, Rio de Janeiro, Brazil
[7]Collège de France, Lab. de Physique Corpusculaire, IN2P3-CNRS, FR-75231 Paris Cedex 05, France
[8]CERN, CH-1211 Geneva 23, Switzerland
[9]Institut de Recherches Subatomiques, IN2P3 - CNRS/ULP - BP20, FR-67037 Strasbourg Cedex, France
[10]Now at DESY-Zeuthen, Platanenallee 6, D-15735 Zeuthen, Germany
[11]Institute of Nuclear Physics, N.C.S.R. Demokritos, P.O. Box 60228, GR-15310 Athens, Greece
[12]FZU, Inst. of Phys. of the C.A.S. High Energy Physics Division, Na Slovance 2, CZ-180 40, Praha 8, Czech Republic
[13]Dipartimento di Fisica, Università di Genova and INFN, Via Dodecaneso 33, IT-16146 Genova, Italy
[14]Institut des Sciences Nucléaires, IN2P3-CNRS, Université de Grenoble 1, FR-38026 Grenoble Cedex, France
[15]Helsinki Institute of Physics, HIP, P.O. Box 9, FI-00014 Helsinki, Finland
[16]Joint Institute for Nuclear Research, Dubna, Head Post Office, P.O. Box 79, RU-101 000 Moscow, Russian Federation
[17]Institut für Experimentelle Kernphysik, Universität Karlsruhe, Postfach 6980, DE-76128 Karlsruhe, Germany
[18]Institute of Nuclear Physics,Ul. Kawiory 26a, PL-30055 Krakow, Poland
[19]Faculty of Physics and Nuclear Techniques, University of Mining and Metallurgy, PL-30055 Krakow, Poland
[20]Université de Paris-Sud, Lab. de l'Accélérateur Linéaire, IN2P3-CNRS, Bât. 200, FR-91405 Orsay Cedex, France
[21]School of Physics and Chemistry, University of Lancaster, Lancaster LA1 4YB, UK
[22]LIP, IST, FCUL - Av. Elias Garcia, 14-1^{o}, PT-1000 Lisboa Codex, Portugal
[23]Department of Physics, University of Liverpool, P.O. Box 147, Liverpool L69 3BX, UK
[24]LPNHE, IN2P3-CNRS, Univ. Paris VI et VII, Tour 33 (RdC), 4 place Jussieu, FR-75252 Paris Cedex 05, France
[25]Department of Physics, University of Lund, Sölvegatan 14, SE-223 63 Lund, Sweden
[26]Université Claude Bernard de Lyon, IPNL, IN2P3-CNRS, FR-69622 Villeurbanne Cedex, France
[27]Dipartimento di Fisica, Università di Milano and INFN-MILANO, Via Celoria 16, IT-20133 Milan, Italy
[28]Dipartimento di Fisica, Univ. di Milano-Bicocca and INFN-MILANO, Piazza della Scienza 2, IT-20126 Milan, Italy
[29]IPNP of MFF, Charles Univ., Areal MFF, V Holesovickach 2, CZ-180 00, Praha 8, Czech Republic
[30]NIKHEF, Postbus 41882, NL-1009 DB Amsterdam, The Netherlands
[31]National Technical University, Physics Department, Zografou Campus, GR-15773 Athens, Greece
[32]Physics Department, University of Oslo, Blindern, NO-0316 Oslo, Norway
[33]Dpto. Fisica, Univ. Oviedo, Avda. Calvo Sotelo s/n, ES-33007 Oviedo, Spain
[34]Department of Physics, University of Oxford, Keble Road, Oxford OX1 3RH, UK
[35]Dipartimento di Fisica, Università di Padova and INFN, Via Marzolo 8, IT-35131 Padua, Italy
[36]Rutherford Appleton Laboratory, Chilton, Didcot OX11 OQX, UK
[37]Dipartimento di Fisica, Università di Roma II and INFN, Tor Vergata, IT-00173 Rome, Italy
[38]Dipartimento di Fisica, Università di Roma III and INFN, Via della Vasca Navale 84, IT-00146 Rome, Italy
[39]DAPNIA/Service de Physique des Particules, CEA-Saclay, FR-91191 Gif-sur-Yvette Cedex, France
[40]Instituto de Fisica de Cantabria (CSIC-UC), Avda. los Castros s/n, ES-39006 Santander, Spain
[41]Inst. for High Energy Physics, Serpukov P.O. Box 35, Protvino, (Moscow Region), Russian Federation
[42]J. Stefan Institute, Jamova 39, SI-1000 Ljubljana, Slovenia and Laboratory for Astroparticle Physics,
Nova Gorica Polytechnic, Kostanjeviska 16a, SI-5000 Nova Gorica, Slovenia,
and Department of Physics, University of Ljubljana, SI-1000 Ljubljana, Slovenia
[43]Fysikum, Stockholm University, Box 6730, SE-113 85 Stockholm, Sweden
[44]Dipartimento di Fisica Sperimentale, Università di Torino and INFN, Via P. Giuria 1, IT-10125 Turin, Italy
[45]INFN,Sezione di Torino, and Dipartimento di Fisica Teorica, Università di Torino, Via P. Giuria 1,
IT-10125 Turin, Italy
[46]Dipartimento di Fisica, Università di Trieste and INFN, Via A. Valerio 2, IT-34127 Trieste, Italy
and Istituto di Fisica, Università di Udine, IT-33100 Udine, Italy
[47]Univ. Federal do Rio de Janeiro, C.P. 68528 Cidade Univ., Ilha do Fundão BR-21945-970 Rio de Janeiro, Brazil
[48]Department of Radiation Sciences, University of Uppsala, P.O. Box 535, SE-751 21 Uppsala, Sweden
[49]IFIC, Valencia-CSIC, and D.F.A.M.N., U. de Valencia, Avda. Dr. Moliner 50, ES-46100 Burjassot (Valencia), Spain
[50]Institut für Hochenergiephysik, Österr. Akad. d. Wissensch., Nikolsdorfergasse 18, AT-1050 Vienna, Austria
[51]Inst. Nuclear Studies and University of Warsaw, Ul. Hoza 69, PL-00681 Warsaw, Poland
[52]Fachbereich Physik, University of Wuppertal, Postfach 100 127, DE-42097 Wuppertal, Germany
† deceased

1 Introduction

Decays $b \to \bar{c}$ are expected to occur through the Cabibbo favoured transitions $b \to cW^-$ and $W^- \to \bar{c}s$ [1]. Hence, neglecting $b \to u$ transition and D^0 mixing, b-hadron decays to wrong sign charmed mesons are in fact double charm transitions. The double charm rate is related to n_c, the mean number of charm quarks (and anti-quarks) produced per b-decay:

$$n_c = 1 - \mathcal{B}(b \to \text{no open charm}) + 2\mathcal{B}(b \to \text{charmonium}) + \mathcal{B}(b \to \text{double charm}) \quad (1)$$

which can be predicted by Heavy Quark Effective Theory (HQET) based calculations of the semileptonic B meson branching fraction [1].

Evidence for wrong sign charm production and double charmed b-decays has been found both at the $\Upsilon(4S)$ and at LEP. ARGUS [2] and CLEO [3] have shown evidence for the two-body transitions $B \to D_s^{(*)+}\bar{D}^{(*)}$ [2]. From the analysis of the D_s momentum spectrum, these decays are found to contribute about half of the total D_s production at the $\Upsilon(4S)$, the remainder coming from either $B \to D_s^{(*)+}\bar{D}^{**}$ or $B \to D_s^{(*)+}\bar{D}^{(*)}\pi, \rho, \omega$ (where D^{**} denotes an orbitally excited D meson). By using D-lepton correlations, CLEO has observed wrong sign D production [4]. ALEPH has reported evidence for $b \to D\bar{D}_{(s)}X$ decays with both charmed mesons reconstructed [5]. The observed $D\bar{D}X$ signal is shown to originate either from $B \to D^{(*)}\bar{D}^{(*)}K^{(*)}$ or from $B \to D_s^{**}\bar{D}$ with a subsequent decay of the orbitally excited state D_s^{**} into $D^{(*)}K$.

In this paper, the DELPHI data are used to measure the inclusive branching fractions of b-hadrons into wrong sign charm mesons, $\mathcal{B}(b \to \bar{D}X)$ and $\mathcal{B}(b \to D_s^- X)$. D^0, D^+ and D_s^+ mesons are exclusively reconstructed in $Z \to b\bar{b}$ events, recorded by DELPHI in the years 1994 and 1995. The wrong sign contribution is extracted by using two discriminant variables: the charge of the b-quark at decay time, estimated from the charges of identified particles, and the momentum of the charmed meson in the rest frame of the b-hadron.

2 Experimental procedure

2.1 The DELPHI detector

A detailed description of the DELPHI detector and its performance can be found in reference [6]. Only the subdetectors relevant to the present analysis are described in the following.

The tracking of charged particles in the barrel region is accomplished with a set of cylindrical tracking detectors whose axes are oriented along the 1.23 T magnetic field and the direction of the beam.

The Time Projection Chamber (TPC), the main tracking device, is a cylinder of 30 cm inner radius, 122 cm outer radius and a length of 2.7 m. For polar angles between 39° and 141°, it provides up to 16 space points along the charged particle trajectory [3].

The Vertex Detector (VD), located nearest to the LEP interaction region, consists of three concentric layers of silicon microstrip detectors at average radii of 6.3 cm, 9.0 cm and 10.9 cm. Since 1994, the innermost and the outermost layers were equipped with double sided silicon microstrip modules allowing both $R\phi$ and z measurements.

[1] Charge conjugate reactions are implied throughout this paper.

[2] In the following, D ($D_{(s)}$) denotes either D^0 or D^+ (D^0, D^+ or D_s^+).

[3] In the DELPHI frame, the z axis is defined along the electron beam direction, the x axis points towards the centre of the LEP ring and the y axis points upwards. The polar angle to the z axis is called θ; the azimuthal angle around the z axis is referred to as ϕ. The radial coordinate is $R = \sqrt{x^2 + y^2}$.

Hadrons are identified using the specific ionization ($\mathrm{d}E/\mathrm{d}x$) measured in the TPC and the Cherenkov radiation detected in the barrel Ring Imaging CHerenkov counter (RICH) placed between the TPC and the Outer Detector (OD).

2.2 Event sample

For this analysis, the data collected by the DELPHI experiment in the years 1994 and 1995 at $\sqrt{s}$ close to 91.2 GeV are used, corresponding to about 2.1 million hadronic Z decays. Simulated hadronic events are generated with the JETSET 7.3 program [7]. Full detector simulation is applied to Monte Carlo events which are subsequently processed through the same analysis chain as the real data [6].

The decays $B \to D_s^{(*)+}\bar{D}^{(*)}$, $B \to D_s^{(*)+}\bar{D}^{**}$, $B \to D_s^{(*)+}\bar{D}^{(*)}\pi, \rho, \omega$, $B \to D_s^{**}\bar{D} \to D^{(*)}K\bar{D}$ and $B \to D^{(*)}\bar{D}^{(*)}K^{(*)}$ are used to model b-decay into wrong sign charmed mesons. The b-hadron decay properties to right sign charm are adjusted to match the latest experimental values [8]. In total, a sample of about 58,000 $b \to \bar{D}_{(s)}X$ and about 99,000 $b \to D_{(s)}X$ events, with $D_{(s)}$ forced to decay into the modes used in the analysis, has been generated. The background is modelled with about 3.2 million $Z \to q\bar{q}$ and about 1.8 million $Z \to b\bar{b}$ Monte Carlo events.

Hadronic Z decays are selected by requiring at least five charged particles and a total charged energy larger than 12% of the collision energy [6]. The tagging of b-quark jets is based on four discriminant variables, the most important one being the probability for all tracks to originate from the primary interaction vertex, calculated from the track impact parameters with respect to this point [9]. The other variables are defined for jets with a secondary vertex: effective mass of the system of particles attached to the secondary vertex, rapidity of these particles with respect to the jet direction and fraction of the charged energy of the jet included in the secondary vertex. All jet b-tags in the event are combined and the cut on the event probability is chosen such that about 90% of the reconstructed charmed mesons originate from b-hadron decay. Correspondingly, the $Z \to b\bar{b}$ selection efficiency varies between 58% and 74% for the different charm modes.

Each selected event is divided into two hemispheres by the plane orthogonal to the axis of the most energetic jet and passing through the primary interaction point.

2.3 Charmed meson reconstruction

Charged particles are selected as follows: momentum larger than 100 MeV/c, relative error on the momentum measurement smaller than 100% and $R\phi$ (z) impact parameter with respect to the primary interaction vertex smaller than 4 cm (4 cm/$\sin\theta$).

Charmed mesons are searched for in the decay modes $D^0 \to K^-\pi^+$, $D^+ \to K^-\pi^+\pi^+$ and $D_s^+ \to \phi\pi^+ \to K^+K^-\pi^+$ by trying all possible combinations of charged particles in the hemisphere. The $\mathrm{d}E/\mathrm{d}x$ values of the kaon and pion candidates are required to be consistent with the respective mass hypotheses. For $D^+ \to K^-\pi^+\pi^+$ decays which suffer from a high level of combinatorial background, the kaon must be tagged additionally by the RICH. To allow for a precise reconstruction of the $D_{(s)}$ decay vertex, at least two tracks in each combination are required to have associated hits in the Vertex Detector.

Track combinations satisfying these criteria are fitted to a common vertex. The χ^2-probability of the fit must exceed 0.01%. Combinations containing a fragmentation track are rejected by requiring the D (D_s) vertex to lie at least three (two) standard deviations away from the primary interaction point and imposing the requirement $x_E > 0.15$ on the

energy fraction $x_E = E_{D_{(s)}}/E_{beam}$. For $D_s^+ \to \phi\pi^+$, a selection at ± 12 MeV/c^2 around the nominal ϕ mass is applied to the reconstructed K^+K^- mass.

D candidates are selected by using four discriminant variables: the RICH information for the kaon candidate, the decay length from the primary to the charm vertex divided by its error, the energy fraction x_E and the cosine of the charm decay angle θ_D, defined as the angle between the K momentum vector in the D meson rest frame and the D momentum vector in the laboratory frame. The $\cos\theta_D$ distribution is flat for the signal and peaked at -1 for the combinatorial background. For D_s candidates, two additional variables are used: the reconstructed K^+K^- mass and the cosine of the ϕ helicity angle θ_H. The latter is defined as the angle between the K^+ and the D_s direction in the ϕ rest frame. The signal follows a $\cos^2\theta_H$ distribution while the background is flat in $\cos\theta_H$. The different variables x_i are combined by using a likelihood ratio:

$$X(D_{(s)}) = \frac{R(D_{(s)})}{1 + R(D_{(s)})} \ , \quad R(D_{(s)}) = \prod_i \frac{S_i(x_i; D_{(s)})}{B_i(x_i; D_{(s)})} \tag{2}$$

where S_i and B_i are the normalised distributions of x_i for the signal and the combinatorial background, respectively, as obtained from the simulation. The combined variable is defined such that the target value is $X = 1$ for the signal and $X = 0$ for the background. For each decay mode, the selection cut on the variable X is adjusted on simulated events to optimise the statistical significance of the signal. The following selections are found: $X(D^0) > 0.8$, $X(D^+) > 0.6$ and $X(D_s) > 0.95$.

For each selected candidate, the invariant mass of the track combination is computed (Figure 1). 7345 (6906, 984) D^0 (D^+, D_s) candidates are found in the signal window corresponding to an interval of about $\pm 2\sigma$ around the signal peak. The remaining combinatorial background is determined by a fit to the invariant mass distribution. The fit uses a Gaussian function for the signal and a linear parametrisation for the combinatorial background. The satellite peak, due to the $D^+ \to K^+K^-\pi^+$ decay, in the $D_s^+ \to \phi\pi^+$ channel is also fitted by a Gaussian function. In this way, the combinatorial background is found to be 3038 ± 43, 4677 ± 66 and 404 ± 12 for $D^0 \to K^-\pi^+$, $D^+ \to K^-\pi^+\pi^+$ and $D_s^+ \to \phi\pi^+$, respectively.

2.4 Discriminant variables

The discriminant variables used for selecting wrong sign decays are constructed by using a common DELPHI analysis package called BSAURUS. Details on how the different BSAURUS variables are formed can be found in reference [10].

The flavour of the $D_{(s)}$ meson, *i.e.*, the charge of the c-quark confined in the charmed meson, is determined from the charge of the kaon for the channels $D^0 \to K^-\pi^+$ and $D^+ \to K^-\pi^+\pi^+$, and from the charge of the pion for the channel $D_s^+ \to \phi\pi^+$.

The charge of the b-quark at decay time in the hemisphere of the charmed meson is obtained from the BSAURUS Decay Flavour Neural Network (BDFNN). The approach is to first form the weighted sum of particle charges in the hemisphere excluding the particles from the exclusive decay of the $D_{(s)}$, in order to avoid a possible bias. The weighting factor is constructed from the conditional probability for the track to have the same charge as the decaying b-quark, and is determined via a neural network technique based mainly on particle identification variables for kaons, protons, electrons and muons and $B-D$ vertex separation variables. In order to use optimally the event information, the resulting hemisphere charges are constructed separately to estimate the b-charge at both production and decay time and this is repeated for each of the b-hadron types (B^+, B^0, B_s^0, b-baryon).

In a final step, these hemisphere charges form the main input variables to a neural network trained to find the b-quark charge in combination with BSAURUS b-hadron type tagging probabilities and also including charge correlation information from the opposite hemisphere.

The wrong sign tag $Y(D_{(s)})$, the first discriminant variable, is obtained by correlating the BDFNN output with the flavour of the charmed meson:

$$Y(D_{(s)}) = \begin{cases} \text{BDFNN} & \text{for } D_{(s)} \\ 1 - \text{BDFNN} & \text{for } \bar{D}_{(s)} \end{cases} . \tag{3}$$

The target values of the BSAURUS Decay Flavour Neural Network are BDFNN = 1 and BDFNN = 0 for b and $\bar{b}$-hadrons, respectively. Hence, the target value of the wrong sign tag is $Y = 0$ for wrong sign decays and $Y = 1$ for right sign.

While wrong sign and B_s right sign decays contribute about equally to the D_s production in $Z \to b\bar{b}$ events, the wrong sign production mechanism is strongly suppressed in the case of D mesons. Hence, for selecting wrong sign D^0 and D^+ mesons, stronger discrimination is required and a second variable, the momentum of the D meson in the b-hadron rest frame, $p(D)$, is used.

The b-hadron four-momentum in the hemisphere of the charmed meson is inclusively reconstructed in BSAURUS using the following procedure. An initial estimate of the b-hadron momentum $\vec{p}_{raw}$, energy E_{raw} and mass $m_{raw} = \sqrt{E_{raw}^2 - p_{raw}^2}$ is formed from particles with high rapidity for events with more than two-jets and from the sum of "b-weighted" four-vectors for the two-jet case. This weighting involves the use of neural networks trained to identify tracks originating from the weakly decaying b-hadron in the hemisphere. E_{raw} is then corrected, hemisphere-by-hemisphere, motivated by the observation (in Monte Carlo simulation) of a correlation between the energy residuals $\Delta E = E_{raw} - E_{true}$ and m_{raw} (which is approximately linear in m_{raw}) and a further correlation between ΔE and $x_h = E_{hem}/E_{beam}$, where E_{hem} is the sum of the energies of all particles reconstructed in the hemisphere, resulting from neutral energy losses and inefficiencies. These effects are parametrised and corrected for, after which the resolution obtained in $p(D)$ is about ± 300 MeV/c.

The two discriminant variables are shown in Figure 2.

2.5 The fit

For each charm decay mode, the numbers of wrong sign and right sign events, N_W and N_R, are determined by a fit to the above-mentioned discriminant variables. The following components can contribute to the distributions of these variables in the real data: wrong sign $b \to \bar{D}_{(s)}X$ mesons, right sign $b \to D_{(s)}X$ mesons, $D_{(s)}$ meson background (contamination by charmed mesons produced in $Z \to c\bar{c}$ events) and combinatorial background. The shapes of the distributions of these four components (F^W, F^R, $F^{c\bar{c}}$ and F^{Bkgrd}) are determined from the Monte Carlo simulation. In each fit, the number of charmed mesons from $Z \to c\bar{c}$ events is fixed to the value calculated from the partial width $R_c = 0.1702 \pm 0.0034$, the fragmentation probabilities $f(c \to D^0) = 0.552 \pm 0.037$, $f(c \to D^+) = 0.237 \pm 0.016$, $f(c \to D_s) = 0.121 \pm 0.025$ [11] and the acceptance determined from the simulation. The numbers are found to be 436 ± 30, 266 ± 19 and 73 ± 15 for $D^0 \to K^-\pi^+$, $D^+ \to K^-\pi^+\pi^+$ and $D_s^+ \to \phi\pi^+$, respectively. The normalisation of the combinatorial background is fixed to the values quoted in Section 2.3.

Sample	Wrong sign evts.	Right sign evts.	ϵ_W/ϵ_R	$\frac{\mathcal{B}(b\to\bar{D}_{(s)}X)}{\mathcal{B}(b\to D_{(s)},\bar{D}_{(s)}X)}$ (%)
$D^0 \to K^-\pi^+$	383 ± 81	$3,396 \pm 110$	0.92 ± 0.02	$11.0 \pm 2.1 \pm 1.5$
$D^+ \to K^-\pi^+\pi^+$	186 ± 86	$1,811 \pm 101$	0.80 ± 0.03	$11.4 \pm 4.7 \pm 3.5$
$D_s^+ \to \phi\pi^+$	286 ± 42	221 ± 39	1.01 ± 0.03	$56.2 \pm 5.7 \pm 3.3$

Table 1: The fitted numbers of wrong sign and right sign mesons, the relative selection efficiency of wrong sign and right sign mesons and the fraction of wrong sign events in the charm signal. The error on the number of events is purely statistical. The error quoted on ϵ_W/ϵ_R is just that due to Monte Carlo statistics. The first error on the wrong sign fraction is statistical; the second one is the sum of all systematic uncertainties listed in Table 2.

Selected D_s meson candidates are arranged in 10 bins, i, of $Y(D_s)$ (bin width 0.1) and the resulting one-dimensional histogram is fitted by the function:

$$N_i = N_W F_i^W + N_R F_i^R + N_{c\bar{c}} F_i^{c\bar{c}} + N_{Bkgrd} F_i^{Bkgrd} \ . \tag{4}$$

The normalisations $\Sigma_i F_i^W = 1$, $\Sigma_i F_i^R = 1$, $\Sigma_i F_i^{c\bar{c}} = 1$ and $\Sigma_i F_i^{Bkgrd} = 1$ are used. Selected D^0 and D^+ candidates are arranged in 4 bins, i, of $Y(D)$ (bin width 0.25) and 13 bins, j, of $p(D)$ (bin width 200 MeV/c) and the fit function:

$$N_{ij} = N_W F_{ij}^W + N_R F_{ij}^R + N_{c\bar{c}} F_{ij}^{c\bar{c}} + N_{Bkgrd} F_{ij}^{Bkgrd} \tag{5}$$

is used. The fit algorithm accounts for finite Monte Carlo statistics [12] and the total number of selected candidates is used as a constraint. By applying the algorithm to simulated $Z \to q\bar{q}$ events, no significant bias in the fit result is observed.

The results obtained by fitting the real data are shown in Figures 3, 5 and 6. The Monte Carlo model of the combinatorial background is tested on real data $D_{(s)}$ candidates selected outside the signal mass window (Figure 4). The numbers of wrong sign and right sign events for each decay channel are given in Table 1. For the one-dimensional fit, the value of the χ^2 is 4.8 compared to $10-1$ degrees of freedom. The two-dimensional fit has $52-1$ degrees of freedom and the χ^2 is 52.0 (62.3) for the D^0 (D^+) sample.

3 Results and systematic uncertainties

For each charm decay mode, the fraction of wrong sign events $b \to \bar{D}_{(s)}X$ in the signal $b \to D_{(s)}, \bar{D}_{(s)}X$ is calculated from the numbers of wrong sign and right sign events:

$$\frac{\mathcal{B}(b \to \bar{D}_{(s)}X)}{\mathcal{B}(b \to D_{(s)}, \bar{D}_{(s)}X)} = \frac{N_W}{N_W + (\epsilon_W/\epsilon_R)N_R} \ . \tag{6}$$

The results are given in Table 1. The factor ϵ_W/ϵ_R in the denominator of Eq. 6 corrects for the different selection efficiencies of wrong sign and right sign mesons and was obtained from the simulation.

The wrong sign charm model used for the fit assumes a 50% contribution of two-body decays $B \to D_s^{(*)+}\bar{D}^{(*)}$ to the wrong sign D_s signal and the same relative contribution of $B \to D_s^{**}\bar{D}$ to wrong sign D. The corresponding modelling uncertainty (Table 2) is estimated by varying these ratios within $(50 \pm 13)\%$ and $(50 \pm 25)\%$, respectively.

Source	Value	$\Delta\frac{\mathcal{B}(b\to\bar{D}^0X)}{\mathcal{B}(b\to D^0,\bar{D}^0X)}$ (%)	$\Delta\frac{\mathcal{B}(b\to D^-X)}{\mathcal{B}(b\to D^\pm X)}$ (%)	$\Delta\frac{\mathcal{B}(b\to D_s^-X)}{\mathcal{B}(b\to D_s^\pm X)}$ (%)	Ref.
Model dependence (w.s.)					
$B \to D_s^{**}\bar{D}$ fraction	$(50 \pm 25)\%$	0.12	1.15		[5,13]
$B \to D_s^{(*)+}\bar{D}^{(*)}$ fraction	$(50 \pm 13)\%$			0.54	[2,3]
Model dependence (r.s.)					
$\mathcal{B}(b \to D^0 l^- \bar{\nu} X)$	$(6.60 \pm 0.60)\%$	0.20			[14]
$\mathcal{B}(b \to D^+ l^- \bar{\nu} X)$	$(2.02 \pm 0.29)\%$		0.61		[14]
$\mathcal{B}(b \to D_s^+ l^- \bar{\nu} X)$	$(0.87 \pm 0.28)\%$			0.61	[8]
$\mathcal{B}(b \to D^0 D_s^- X)$	$(9.10 \pm 3.35)\%$	0.08			[5]
$\mathcal{B}(b \to D^+ D_s^- X)$	$(4.00 \pm 2.05)\%$		0.59		[5]
$\mathcal{B}(b \to D_s^+ D_s^- X)$	$(1.17 \pm 0.71)\%$			2.09	[5]
$\mathcal{B}(b \to D^0 \bar{D} X)$	$(6.45 \pm 2.08)\%$	1.40			[5]
$\mathcal{B}(b \to D^+ \bar{D} X)$	$(1.80 \pm 0.96)\%$		2.18		[5]
$\mathcal{B}(b \to D_s^+ \bar{D} X)$	$(1.17 \pm 0.71)\%$			2.39	
$Z \to c\bar{c}$ background		0.09	0.05	0.56	
Combinatorial background					
normalisation		0.37	1.46	0.29	
shape			1.56		
ϵ_W/ϵ_R		0.41	1.04	0.13	
Total		1.53	3.53	3.34	

Table 2: Breakdown of the systematic error on the wrong sign fractions. For the total, the different components have been added in quadrature.

The different decays used to model the right sign component are collected into four categories: $b \to D_{(s)} l^- \bar{\nu}_l(X)$, $b \to D_{(s)}\pi, \rho, \omega, \ldots$, $b \to D_{(s)} D_s^-(X)$ and $b \to D_{(s)}\bar{D}(X)$. To estimate the systematics related to the right sign modelling, the relative contributions of $b \to D_{(s)} l^- \bar{\nu}_l(X)$, $b \to D_{(s)} D_s^-(X)$ and $b \to D_{(s)}\bar{D}(X)$ to the signal are varied. The ranges are obtained from recent measurements (Table 2). The weight of each category is varied separately and, for the total, the different contributions are added in quadrature.

Further contributions to the systematic error are: normalisation of the $Z \to c\bar{c}$ background (uncertainty in R_c and in the fragmentation probabilities), normalisation of the combinatorial background (uncertainty of the fit to the invariant mass distribution) and uncertainty in ϵ_W/ϵ_R. For the $D^+ \to K^-\pi^+\pi^+$ sample which is particularly affected by the combinatorial background, instead of using simulated data in the signal window, the fit is repeated using real data candidates selected outside the signal window. Both approaches are statistically consistent and the difference in the fit result is interpreted as a systematic uncertainty related to the combinatorial background shape.

4 Conclusion

The production of wrong sign charm mesons in b-hadron decay, $b \to \bar{D}_{(s)}X$, $D_{(s)} = (D^0, D^+, D_s)$, was studied using the DELPHI data collected in 1994 and 1995, leading to a measurement of the fraction $\mathcal{B}(b \to \bar{D}_{(s)}X)/\mathcal{B}(b \to D_{(s)}, \bar{D}_{(s)}X)$. Combining this measurement with the branching fractions $\mathcal{B}(b \to D^0, \bar{D}^0X) = (60.5 \pm 3.2)\%$, $\mathcal{B}(b \to D^{\pm}X) = (23.7 \pm 2.3)\%$ and $\mathcal{B}(b \to D_s^{\pm}X) = (18 \pm 5)\%$ [8], the following result is obtained for wrong sign D:

$$\mathcal{B}(b \to \bar{D}^0X) + \mathcal{B}(b \to D^-X) = (9.3 \pm 1.7(stat) \pm 1.3(syst) \pm 0.4(\mathcal{B}))\% \; .$$

The first uncertainty is statistical, the second one is the sum of all systematic errors listed in Table 2 (accounting for correlated model systematics) and the last one corresponds to the uncertainties in $\mathcal{B}(b \to D^0, \bar{D}^0X)$ and $\mathcal{B}(b \to D^{\pm}X)$ (note that the quoted statistical error includes both real data and Monte Carlo statistics). This value is in good agreement with previous measurements by CLEO [4] and ALEPH [5]. The inclusive branching fraction for wrong sign D_s is found to be:

$$\mathcal{B}(b \to D_s^-X) = (10.1 \pm 1.0(stat) \pm 0.6(syst) \pm 2.8(\mathcal{B}))\% \; .$$

Again, the first uncertainty is statistical, the second one is the total systematic error of Table 2 and the last one corresponds to the uncertainty on $\mathcal{B}(b \to D_s^{\pm}X)$. This value agrees with the total D_s production rate at the $\Upsilon(4S)$, $\mathcal{B}(B \to D_s^{\pm}X) = (10.0 \pm 2.5)\%$ [8], where the dominant source of D_s production is double charm b-decay.

Acknowledgements

We are greatly indebted to our technical collaborators, to the members of the CERN-SL Division for the excellent performance of the LEP collider, and to the funding agencies for their support in building and operating the DELPHI detector.
We acknowledge in particular the support of
Austrian Federal Ministry of Education, Science and Culture, GZ 616.364/2-III/2a/98,
FNRS–FWO, Flanders Institute to encourage scientific and technological research in the industry (IWT), Belgium,
FINEP, CNPq, CAPES, FUJB and FAPERJ, Brazil,

Czech Ministry of Industry and Trade, GA CR 202/99/1362,
Commission of the European Communities (DG XII),
Direction des Sciences de la Matière, CEA, France,
Bundesministerium für Bildung, Wissenschaft, Forschung und Technologie, Germany,
General Secretariat for Research and Technology, Greece,
National Science Foundation (NWO) and Foundation for Research on Matter (FOM), The Netherlands,
Norwegian Research Council,
State Committee for Scientific Research, Poland, SPUB-M/CERN/PO3/DZ296/2000 and SPUB-M/CERN/PO3/DZ297/2000
JNICT–Junta Nacional de Investigação Científica e Tecnológica, Portugal,
Vedecka grantova agentura MS SR, Slovakia, Nr. 95/5195/134,
Ministry of Science and Technology of the Republic of Slovenia,
CICYT, Spain, AEN99-0950 and AEN99-0761,
The Swedish Natural Science Research Council,
Particle Physics and Astronomy Research Council, UK,
Department of Energy, USA, DE–FG02–94ER40817.

References

[1] M. Neubert and C. T. Sachrajda, Nucl. Phys. **B483** (1997) 339.
[2] H. Albrecht *et al.* (ARGUS Collaboration), Zeit. Phys. **C54** (1992) 1.
[3] D. Gibaut *et al.* (CLEO Collaboration), Phys. Rev. **D53** (1996) 4734.
[4] T. E. Coan *et al.* (CLEO Collaboration), Phys. Rev. Lett. **80** (1998) 1150.
[5] R. Barate *et al.* (ALEPH Collaboration), Eur. Phys. J. **C4** (1998) 387.
[6] P. Aarnio *et al.* (DELPHI Collaboration), Nucl. Instr. Meth. **A303** (1991) 233;
P. Abreu *et al.* (DELPHI Collaboration), Nucl. Instr. Meth. **A378** (1996) 57.
[7] T. Sjöstrand, Comp. Phys. Comm. **39** (1986) 347;
T. Sjöstrand and M. Bengtsson, Comp. Phys. Comm. **43** (1987) 367.
[8] D. E. Groom *et al.* (Particle Data Group), Eur. Phys. J. **C15** (2000) 1.
[9] P. Abreu *et al.* (DELPHI Collaboration), Eur. Phys. J. **C10** (1999) 415.
[10] T. Allmendinger, G. Barker, M. Feindt, C. Haag, M. Moch, hep-ex/0102001.
[11] "A Combination of Preliminary Electroweak Measurements and Constraints on the Standard Model", the LEP Collaborations, the LEP Electroweak Working Group, and the SLD Heavy Flavour and Electroweak Group, preprint CERN-EP/2001-021.
[12] R. Barlow, C. Beeston, J. Comp. Phys. **72** (1987) 202.
[13] M. Bishai *et al.* (CLEO Collaboration), Phys. Rev. **D57** (1998) 3847.
[14] R. Akers *et al.* (OPAL Collaboration), Z. Phys. **C67** (1995) 57.

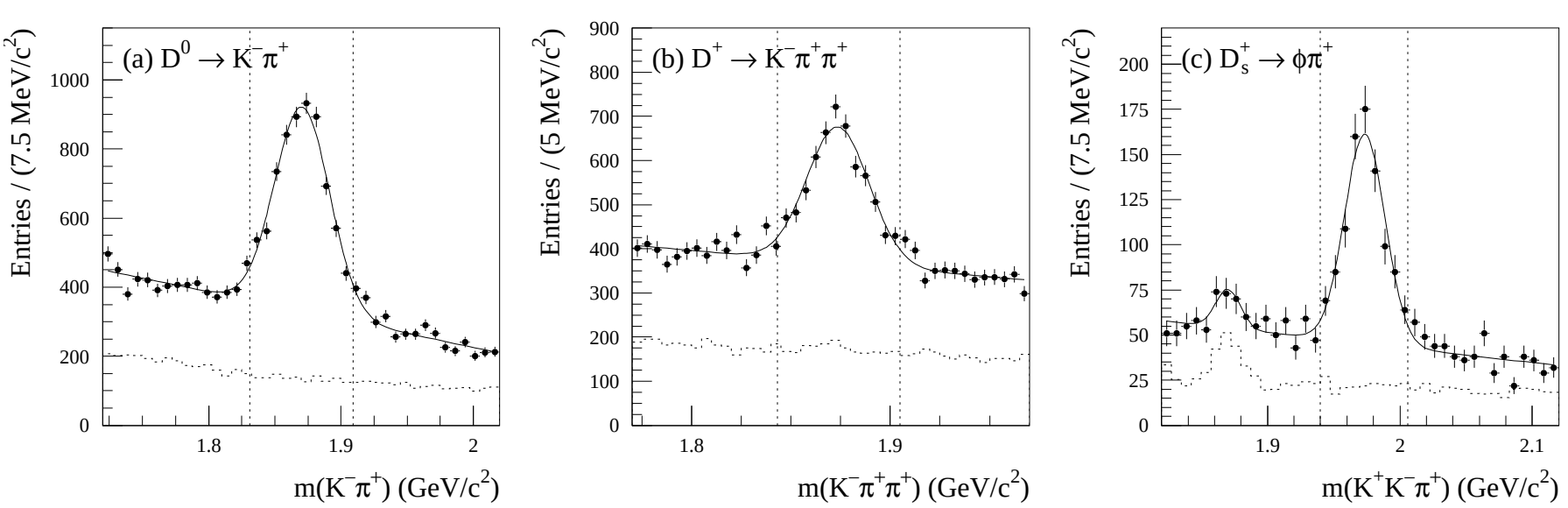

Figure 1: The invariant mass of selected $D^0 \to K^-\pi^+$, $D^+ \to K^-\pi^+\pi^+$ and $D_s^+ \to \phi\pi^+ \to K^+K^-\pi^+$ candidates. The points with error bars are the real data. The solid line is the result of the fit mentioned in the text. The signal window is shown by dashed vertical lines and the dashed histogram represents the Monte Carlo expectation for the combinatorial background (arbitrary normalisation).

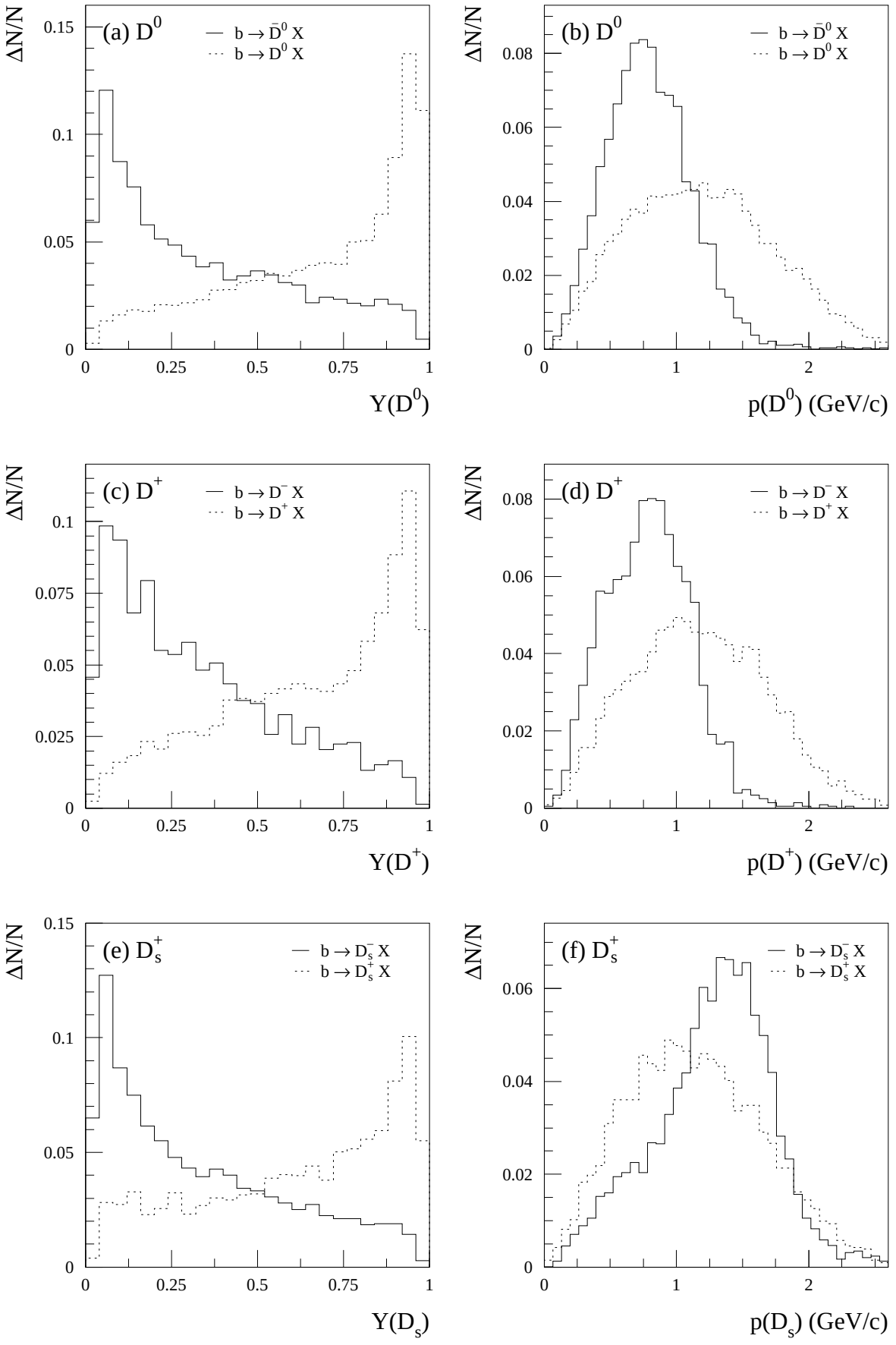

Figure 2: The wrong sign tag $Y(D_{(s)})$ and the momentum of the charmed meson in the rest frame of the b-hadron $p(D_{(s)})$, shown for wrong sign and right sign Monte Carlo

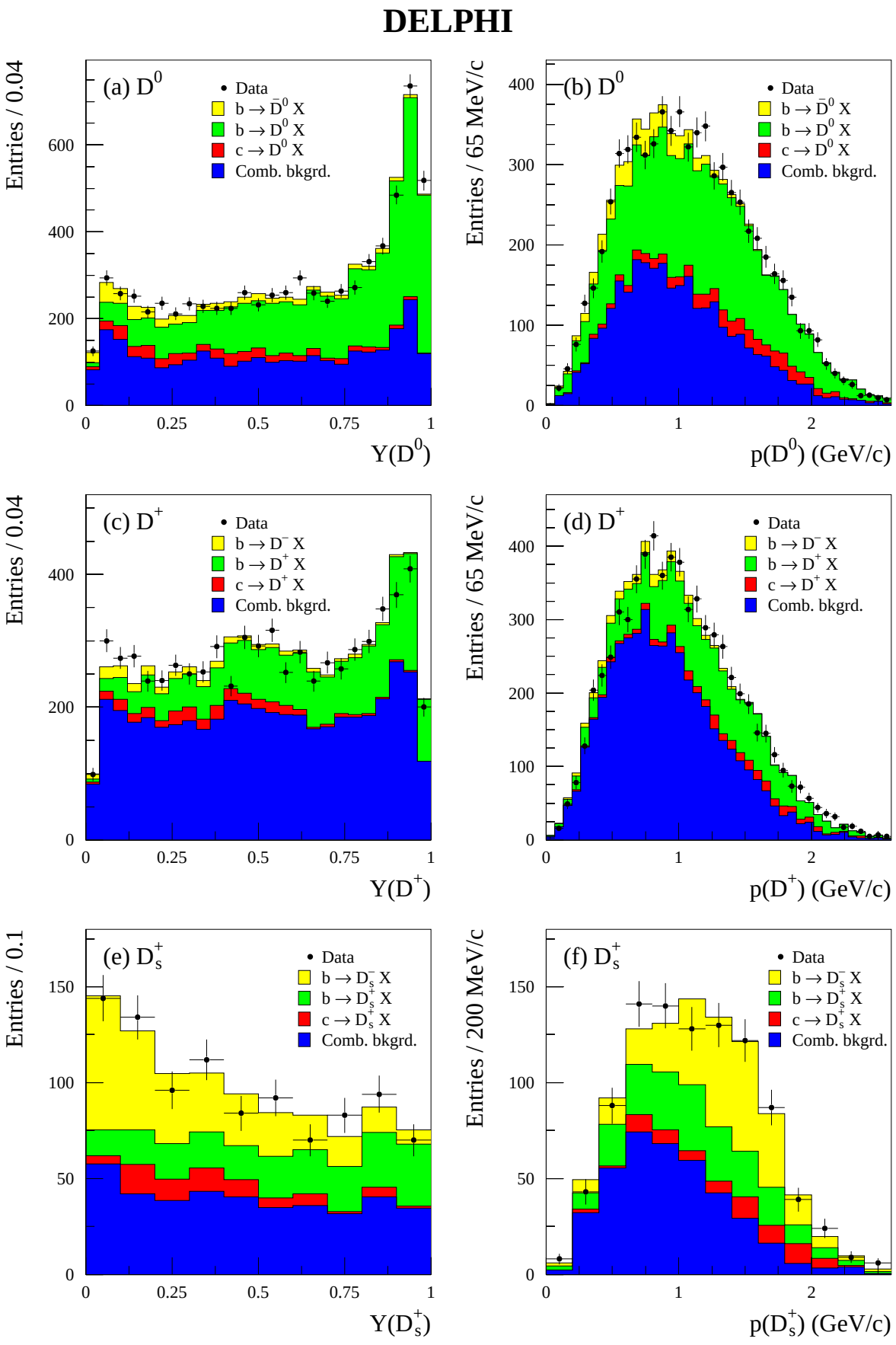

Figure 3: The wrong sign tag $Y(D_{(s)})$ and the momentum of the charmed meson in the rest frame of the b-hadron $p(D_{(s)})$. The data are the points with error bars; the

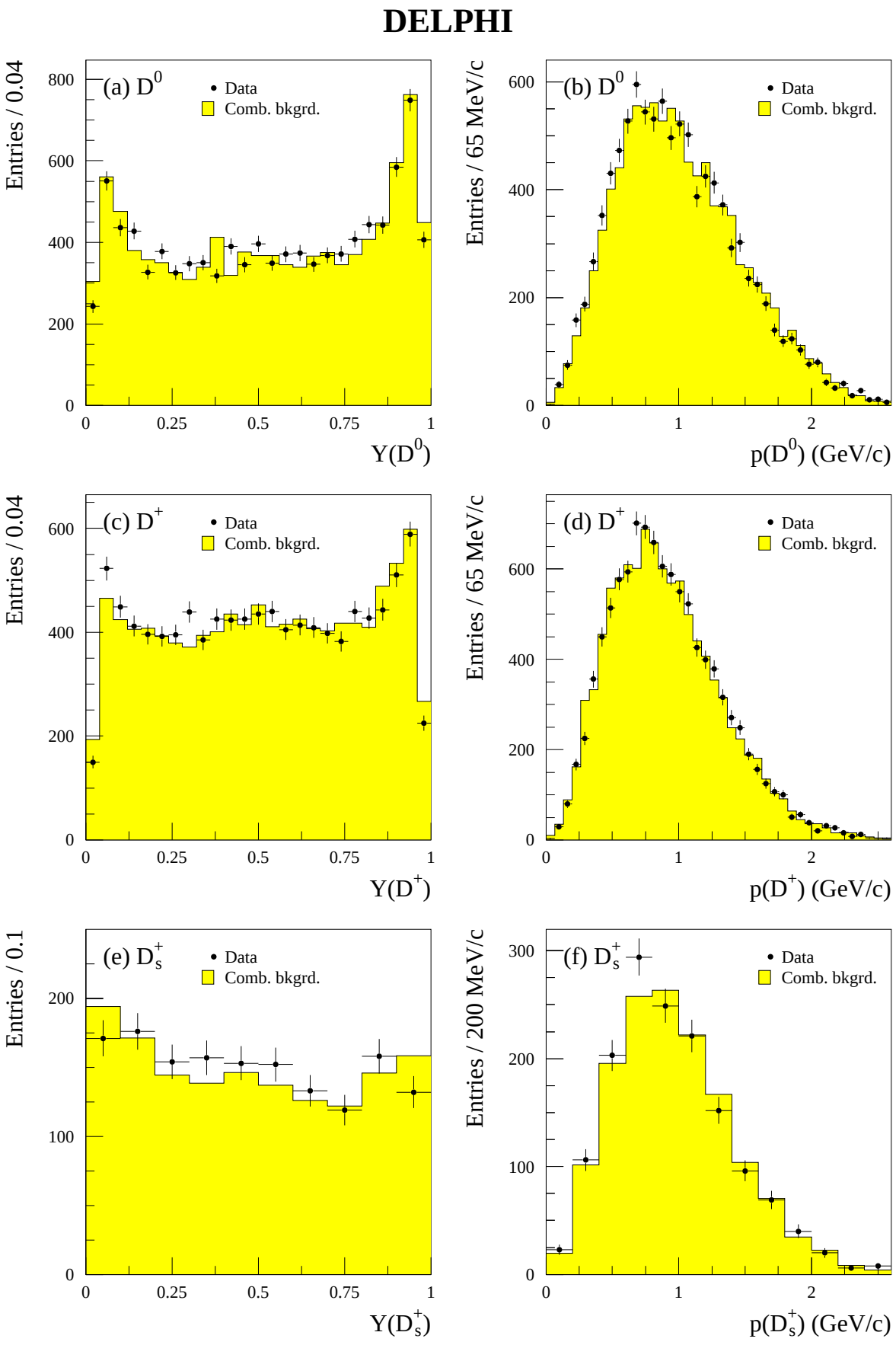

Figure 4: Same as Figure 3 for candidates selected outside the signal mass window.

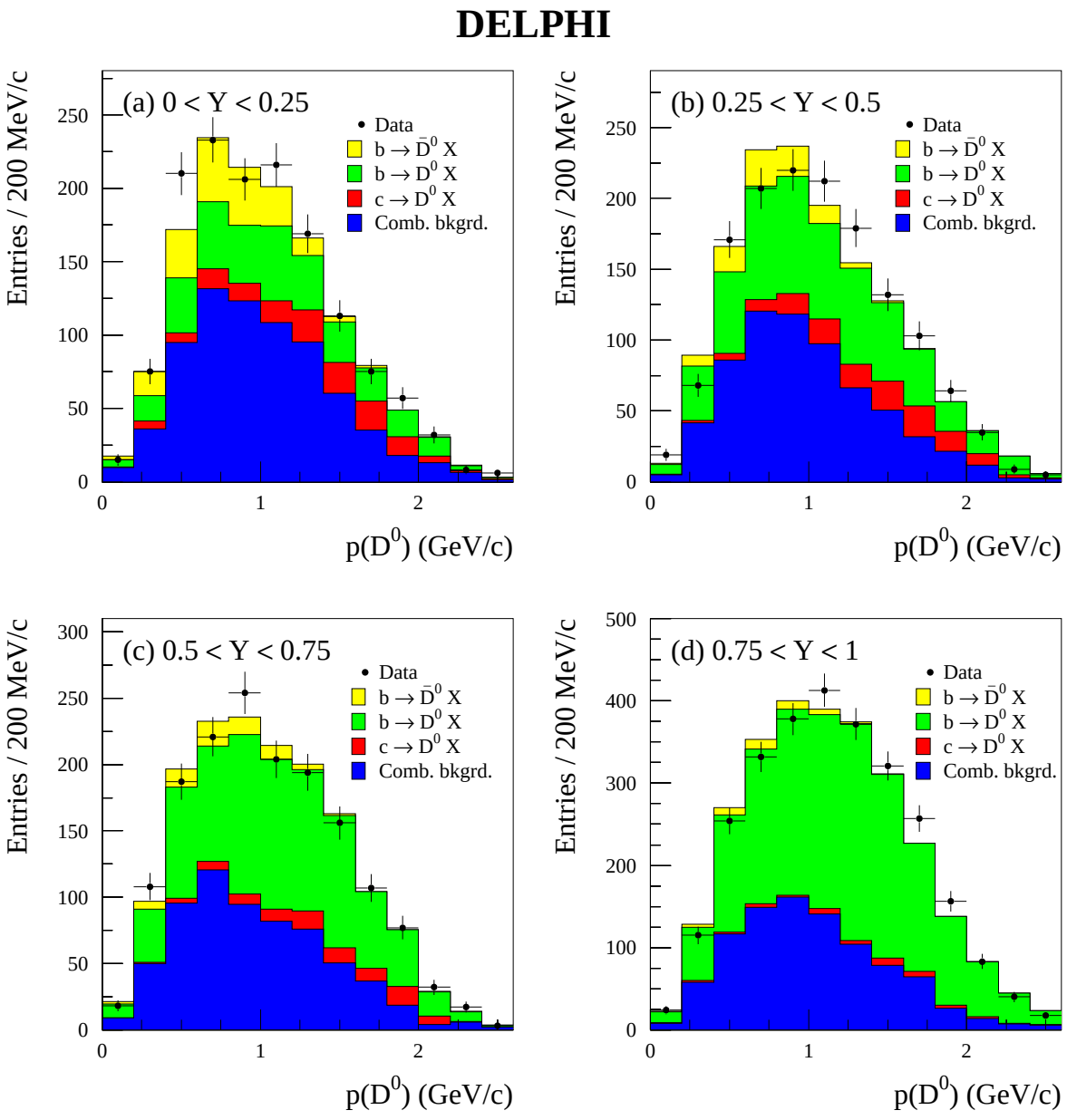

Figure 5: The D^0 momentum in the b-hadron rest frame $p(D^0)$ in bins of the wrong sign tag $Y(D^0)$. The data are the points with error bars; the histograms are the components of the fit function (as described in the text).

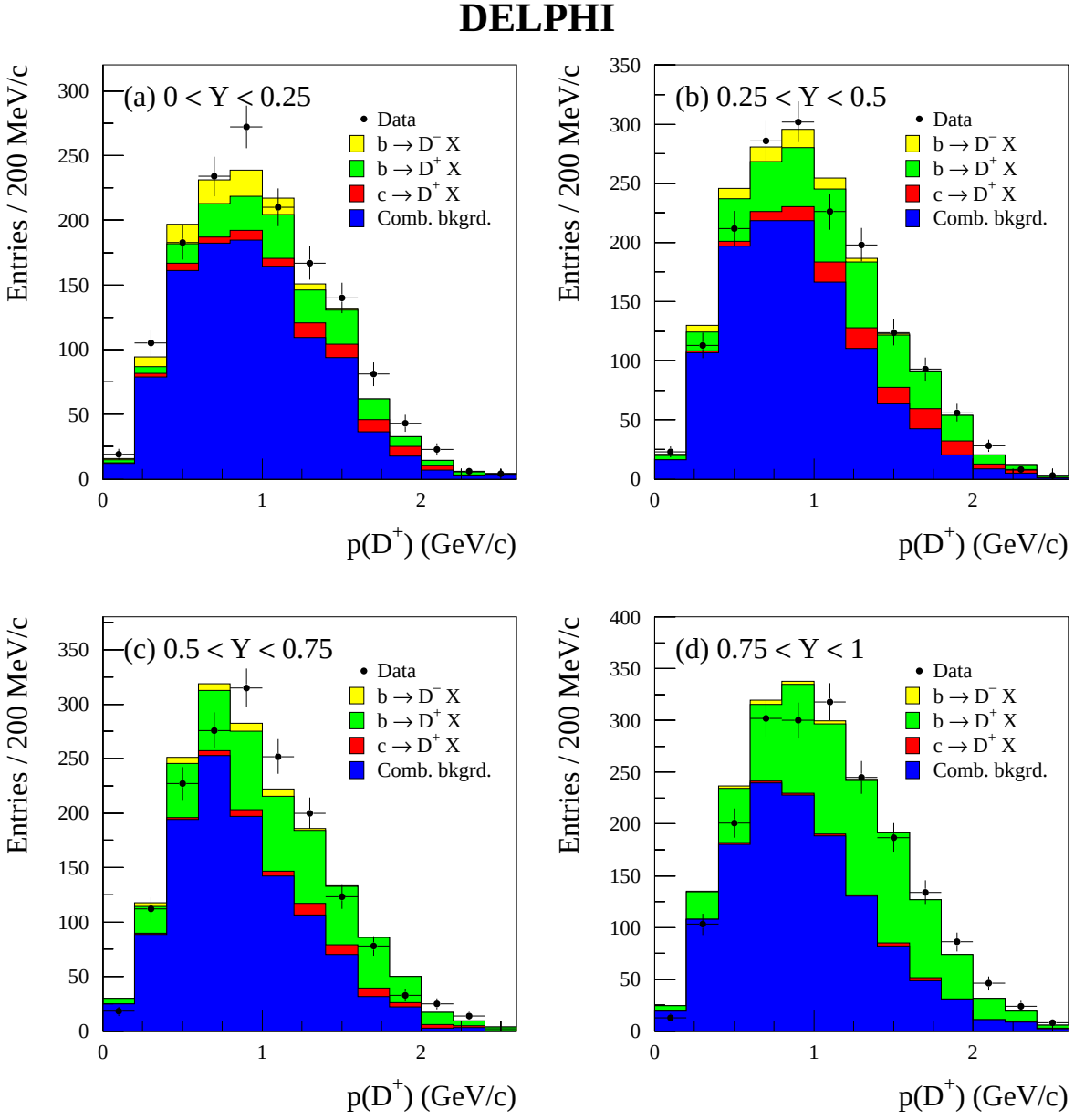

Figure 6: Same as Figure 5 for D^+.